DMD Fast Forward. Published on March 24, 2006 as doi:10.1124/dmd.105.009209

N-methylpurine DNA glycosylase and 8-oxoguanine DNA glycosylase metabolize the antiviral nucleoside 2-bromo-5,6-dichloro-1-(β-D-ribofuranosyl)benzimidazole

Philip L. Lorenzi[1], Christopher P. Landowski[2], Andrea Brancale, Xueqin Song, Leroy B. Townsend, John C. Drach and Gordon L. Amidon.

Department of Pharmaceutical Sciences (P.L.L., C.P.L., X.S., G.L.A.) and Medicinal Chemistry (L.B.T., J.C.D.), College of Pharmacy, and Department of Biologic and Materials Sciences (J.C.D.), School of Dentistry, University of Michigan, Ann Arbor, Michigan, USA; and Welsh School of Pharmacy (A.B.), Cardiff University, Wales, UK.

Running Title: Nucleoside drug metabolism by DNA repair enzymes

Text pages: 19
Tables: 4
Figures: 3
References: 43
Words in Abstract: 180
Words in Introduction: 464
Words in Discussion: 1433

Abbreviations: BDCRB, 2-bromo-5,6-dichloro-1-(β-D-ribofuranosyl)benzimidazole; TCRB, 2,5,6-trichloro-1-(β-D-ribofuranosyl)benzimidazole; maribavir, 5,6-dichloro-2-(isopropylamino)-1-β-L-ribofuranosyl-1H-benzimidazole; FTCRI, 3-formyl-2,5,6-trichloro-1-(β-D-ribofuranosyl)indole; HCMV, human cytomegalovirus; DMEM, Dulbecco's Modified Eagle Medium; PBS, phosphate buffered saline; NRS, NADPH-regenerating system; LOD, limit of detection; OGG1, 8-oxoguanine DNA glycosylase; MPG, N-methylpurine DNA glycosylase; PNP, purine nucleoside phosphorylase; TP, thymidine phosphorylase; TGT, tRNA-guanine transglycosylase; HPLC, high performance liquid chromatography; MD, molecular dynamics

Corresponding Author: Gordon L. Amidon, Ph.D.
Department of Pharmaceutical Sciences
College of Pharmacy
University of Michigan
428 Church Street
Ann Arbor MI 48109-1065
Tel: 734-764-2464
Fax: 734-763-6423
E-mail: glamidon@umich.edu

Abstract

The rapid *in vivo* degradation of the potent HCMV inhibitor BDCRB compared to a structural L-analog, maribavir, has been attributed to selective glycosidic bond cleavage. An enzyme responsible for this selective BDCRB degradation, however, has not been identified. Here, we report the identification of two enzymes, 8-oxoguanine DNA glycosylase (OGG1) and N-methylpurine DNA glycosylase (MPG), that catalyze N-glycosidic bond cleavage of BDCRB and its 2-chloro homolog, TCRB, but not maribavir. To our knowledge, this is the first demonstration that free nucleosides are substrates of OGG1 and MPG. To understand how these enzymes might process BDCRB, docking and molecular dynamics simulations were performed with the native hOGG1 crystal coordinates. These studies showed that OGG1 was not able to bind a negative control, guanosine, yet BDCRB and maribavir were stabilized through interactions with various binding site residues, including Phe^{319}, His^{270}, Ser^{320}, and Asn^{149}. Only BDCRB, however, achieved orientations whereby its anomeric carbon, C1′, could undergo nucleophilic attack by the putative catalytic residue, Lys^{249}. Thus, *in silico* observations were in perfect agreement with experimental observations. These findings implicate DNA glycosylases in drug metabolism.

Introduction

Human cytomegalovirus (HCMV), a member of the *Herpesviridae* family of viruses, infects up to 95% of all adults in the United States by age 40. Though no associated symptoms or long-term health consequences generally arise, HCMV infection can cause serious disease or death in immunocompromised patients such as organ transplant recipients or those with HIV. The poor bioavailability, toxicity, and high potential for cross-resistance of the current line of HCMV therapy continue to spur development of new and improved antiviral agents.

Benzimidazole D-ribonucleosides such as BDCRB were identified as potent inhibitors of HCMV replication over a decade ago (Townsend and Drach, 1992; Townsend et al., 1995). In addition to excellent potency, BDCRB exhibits low toxicity to uninfected cells due to its viral-specific mechanism of action; BDCRB and its 2-chloro homolog, TCRB, block viral DNA cleavage and packaging (Underwood et al., 1998) through inhibition of the viral terminase encoded by genes UL56 and UL89 (Krosky et al., 1998; Scheffczik et al., 2002; Scholz et al., 2003). Despite these positive attributes, BDCRB was not considered to be a clinical candidate due to extensive glycosidic bond cleavage following oral and intravenous administration to rats and monkeys (Good et al., 1994). This prompted the search for analogs with more stable glycosidic bonds (Chulay et al., 1999; Townsend et al., 1999) that ultimately led to the development of maribavir. This L-ribofuranosyl analog is also a potent inhibitor of HCMV replication (Biron et al., 2002) but has greatly enhanced metabolic stability and bioavailability (Chulay et al., 1999; Koszalka et al., 2002). More recently, we synthesized a series of amino acid prodrugs of BDCRB that demonstrated significantly enhanced metabolic stability *in vitro*

and *in vivo* (Lorenzi et al., 2005). Although susceptibility of BDCRB to glycosidic bond cleavage *in vivo* has been known for some time, there have been no reports on the mechanism responsible for this metabolism. With maribavir as a stable reference compound, we therefore sought to identify enzymes that preferentially catalyze BDCRB glycosidic bond cleavage.

Based upon the greater efficacy of maribavir compared to BDCRB following oral administration to mice (Kern et al., 2004), metabolizing enzymes located in the intestine and liver were of particular interest, especially because such identification could lead to optimization of new drug design. In this report, we describe the *in vitro* stability of BDCRB and maribavir in homogenates of Caco-2 cells, an established model of human intestinal metabolism (Hidalgo et al., 1989), and in human liver microsomes. Gene expression profiling was used to identify expressed human enzymes capable of cleaving N-glycosidic bonds. Five of fifteen identified enzymes were obtained and tested, and two were found to recognize BDCRB as a substrate. Finally, molecular dynamics (MD) simulations provided an explanation for the ability of one of these enzymes to process BDCRB but not maribavir.

Materials and Methods

Materials. BDCRB, its 2-chloro homolog (TCRB), the indole analog 3-formyl-2,5,6-trichloro-1-(β-D-ribofuranosyl)indole (FTCRI) and their aglycones were synthesized in the laboratory of Dr. Leroy B. Townsend. Maribavir (5,6-dichloro-2-(isopropylamino)-1-β-L-ribofuranosyl-1H-benzimidazole, also known as 1263W94) was kindly provided by Dr. Karen K. Biron, GlaxoSmithKline (Research Triangle Park, NC). Human OGG1 (hOGG1) and murine MPG (mMPG) enzymes were purchased from Trevigen, Inc. (Gaithersburg, MD). E. coli tRNA-guanine transglycosylase (TGT) was graciously provided by Dr. George Garcia, College of Pharmacy, University of Michigan. Pooled human liver microsomes were purchased from In-Vitro Technologies. Other natural and modified nucleosides, human purine nucleoside phosphorylase (hPNP) and human thymidine phosphorylase (hTP) were purchased from Sigma (St. Louis, MO). Model U95Av2 GeneChips® were purchased from Affymetrix. All other chemicals were of analytical grade or better. Stock drug solutions were prepared at 100 mM in DMSO.

Metabolism by Caco-2 Cell Homogenates. Passage 34 – 40 Caco-2 cells (ATCC, Manassas, VA) were cultured in Dulbecco's modified Eagle's medium (DMEM) containing 10% fetal bovine serum (FBS), 1% nonessential amino acids, 1mM sodium pyruvate and 1% L-glutamine (all reagents obtained from Invitrogen, Carlsbad, CA). Cultures were grown in an atmosphere of 5% CO_2 and 90% relative humidity at 37^{o}C. Culture dishes were washed with cold PBS and the cells scraped with a rubber policeman into a tube on ice containing 0.5% Triton X-100 in Buffer C: 10 mM HEPES, 25 mM KCl and 5 mM $MgCl_2$ pH 7.4. The cell suspension was incubated at room temperature for 10 min then pipetted up and down for 20 – 30 s to lyse the cells and intracellular

organelles. Greater than 90% homogenization was confirmed via phase contrast microscopy and trypan blue staining. Total protein was determined with the DC Protein Microplate assay (Bio-Rad, Hercules, CA) and BSA standards.

Caco-2 homogenate reaction conditions were optimized through standard enzyme kinetic approaches as previously reported (Birnie et al., 1963). Briefly, BDCRB, maribavir and a positive control for enzyme activity, inosine, were first tested in a study in the presence and absence of approximately 1 mg/mL Caco-2 protein in Buffer C at 37°C. Substrate was added to each homogenate and corresponding negative control at a final concentration of 200 μM, and aliquots taken at 0 and 60 min were quenched in ice-cold methanol. Aglycone was quantitated via HPLC, and the formation rate determined as slope of the line from the 0 to 60 min sample. A compound was considered a substrate if the aglycone accumulation rate was statistically significant relative to the negative control by 2-tailed t-tests and significance level of 0.05.

For compounds determined to undergo enzymatic N-glycosidic bond cleavage, the optimal protein level was next determined by measuring metabolism rate of 1 mM substrate as a function of protein concentration. Following serial dilution of Caco-2 homogenate and addition of drug, an aliquot was taken from each reaction at 20 min, quenched and extracted with ice-cold methanol, filtered through a 96-well Whatman GF/B Uni-filter plate by centrifugation at 400 g for one minute, and analyzed by HPLC. Metabolite appearance rate was plotted as a function of protein concentration, of which a value at the high end of the linear range was chosen for subsequent experiments.

Reaction time was optimized by finding the linear time range of the reaction between 1 mM substrate and the chosen protein concentration. The kinetic parameters

K_m and V_{max} were finally determined using 10 to 12 serially diluted substrate concentrations.

Metabolism by Human Liver Microsomes. Pooled microsomal protein (In Vitro Technologies, Baltimore, MD) was diluted to working concentrations ranging from 1 – 500 μg/mL in 100 mM Tris-HCl, pH 7.4. BDCRB, maribavir, and the positive control, verapamil, were prepared in NADPH Regenerating Solution: final 0.125 mg/mL NADP+, 0.5 mg/mL glucose-6-phosphate, 0.375 U/mL glucose-6-phosphate dehydrogenase and 0.5% $NaHCO_3$ (w/v). These drug solutions were then combined with microsomal protein to yield desired protein and drug concentrations. Reactions were conducted at 150 μg/mL.

Metabolism by Caco-2 Cell Fractions. To localize the enzymatic cleavage of BDCRB's glycosidic bond, Caco-2 cells were fractionated into nuclear and soluble fractions and the BDCRB metabolism kinetics determined. Prior to mechanical shearing of Caco-2 plasma membranes, Buffer C lacking detergent and a 50 mL zero-clearance Potter-Elvehjem homogenizer were placed on ice. Ninety percent confluent Caco-2 cells were washed with PBS then scraped into a 50 mL tube containing 8 mL Buffer C. The cell suspension was homogenized with 60 up-down strokes of the Potter-Elvehjem homogenizer at rotational speed 600 RPM. Cells were transferred into a 15 mL tube with the original volume of buffer. The shorn Caco-2 cell suspension was centrifuged at 600 *g* and 4°C for 10 min to yield the nuclear pellet, which was resuspended in 1 mL of Buffer C containing 0.5% Triton X-100. The supernatant fraction was brought to 0.5% Triton X-100 as well, and both fractions were incubated 10 min before pipetting vigorously to lyse subcellular organelles. Metabolism reactions were then performed and optimized as

above. To confirm the supernatant was not contaminated with nuclear contents, the nuclear and supernatant fractions were blotted onto a Hybond-N+ nucleic acid transfer membrane with DNA standards ranging from 0.01 to 100 μg/mL. After crosslinking with a Spectrolinker XL-1000, the membrane was developed with SYBR Green and visualized with UV. The results showed little DNA in the supernatant fraction (Fig. S3, Supplemental Data).

Gene Expression Profiling. To identify expressed enzymes potentially involved in BDCRB metabolism, twenty two U95Av2 GeneChips® (Affymetrix, Santa Clara, CA) were used to acquire gene expression data as reported previously (Sun et al., 2002) from human intestinal samples. Total RNA from human jejunum (Ambion, Austin, TX), human ileum (Stratagene, La Jolla, CA), and human colon (Clontech, Palo Alto, CA) was purchased commercially. Human duodenal biopsies were acquired as previously described, and Caco-2 cells were grown to 4 days (undifferentiated) and 16 days (differentiated) post-seeding (Sun et al., 2002). Briefly, the tissue and cell samples were homogenized in TRIzol (Gibco BRL, Grand Island, NY), and total RNA was isolated, converted to cDNA, then converted back to biotin-labeled cRNA. The biotin-labeled cRNA was fragmented and hybridized to the GeneChip® together with controls (Bio B, C, D, and Cre). The GeneChip® was then washed and stained with streptavidin phycoerythrin solution. After washing, the GeneChip® was scanned with a laser scanner (Affymetrix). The gene expression profiles from these twenty two samples were analyzed by Affymetrix Microarray Suite (MAS version 5.0) and Data Mining Tool software, and the data have been deposited to the NCBI Gene Expression Omnibus

(GEO, http://www.ncbi.nlm.nih.gov/geo/) under GEO Series accession number GSE1862[3].

A list of potential BDCRB-metabolizing enzymes was generated as follows. Since glycosylases and phosphorylases are the two major enzyme classes known to cleave N-glycosidic bonds, the Affymetrix annotations were first queried for entries containing these two terms in addition to the term "nucleoside," which was intended to capture genes that have not yet been fully annotated or characterized but may code for gene products that possess N-glycosylase activity. Next, the corresponding expression data was queried for entries determined to be statistically present in at least one sample according to the absolute detection call significance level of 0.05. These results were finally filtered down to a small list of fifteen potential enzymes by querying for enzymes reported to act on glycosidic bonds. This final step primarily eliminated entries that were falsely captured by the search term "nucleoside" in the first step. Five of the resulting fifteen enzymes were obtained and experimentally tested for BDCRB metabolism—8-oxoguanine DNA glycosylase (OGG1), N-methylpurine DNA glycosylase (MPG), purine nucleoside phosphorylase (PNP), thymidine phosphorylase (TP) and tRNA-guanine transglycosylase (TGT).

Metabolism by Selected Enzymes. Metabolism reactions were conducted and optimized in the presence of selected enzymes as described above, with 3.0 μg/mL enzyme used for initial studies. The reaction buffer for hOGG1 reactions contained 1 mM DTT, 1 mM EDTA, 20 mM Tris-HCl pH 8.0 and 0.1 mg/mL BSA. The reaction buffer for murine MPG reactions contained 1 mM DTT, 100 mM KCl, 1 mM EDTA and 10 mM HEPES pH 7.4. TGT reaction buffer contained 10 mM $MgCl_2$, 2 mM DTT and

10 mM Tris-HCl pH 7.5. Reaction buffer for both hPNP and hTP contained 100 mM potassium phosphate pH 7.4. MPG and OGG1 purity were determined by SDS-PAGE to be 85-90% and 80-85%, respectively. Inosine and thymidine were included as positive control substrates of hPNP and hTP, respectively. Negative control reactions were conducted in the absence of enzyme for statistical comparison of aglycone generation. The substrate specificity of hOGG1 was investigated by testing several BDCRB analogs, including TCRB, FTCRI and the endogenous nucleosides adenosine, inosine and guanosine. Optimization of BDCRB metabolism reactions as previously described yielded optimal protein concentrations hOGG1 = 3 μg/mL and mMPG = 6 μg/mL, which produced reaction linearity through 8 min (see Supplemental Data). Concentration-dependence studies yielded a plateau in reaction velocity with increasing BDCRB concentration, thereby allowing calculation of K_m and V_{max}.

As stock solutions of all compounds were made in DMSO, the high nucleoside drug concentrations required to saturate OGG1 and MPG in concentration-dependence studies produced 30% DMSO concentrations at 30 mM substrate. Therefore, the effect of DMSO on enzyme activity was assessed by determining the rate of BDCRB aglycone formation at the following substrate and DMSO concentrations in the presence of 3 μg/mL hOGG1: 2 mM BDCRB in 2% DMSO, 2 mM BDCRB in 30% DMSO, 30 mM BDCRB in 2% DMSO and 30 mM BDCRB in 30% DMSO. The reaction was sampled at 8 min and analyzed by HPLC to quantitate aglycone and calculate initial reaction rate. The rates of BDCRB aglycone formation were 7.1 ± 1.0 nmol/min/mg, 6.9 ± 0.8 nmol/min/mg, 10.2 ± 2.7 nmol/min/mg and 41.3 ± 3.5 nmol/min/mg, respectively. These

data indicate that DMSO had little to no effect on enzyme activity at 30% compared to 2%. Data are expressed as mean ± SD for three independent determinations.

HPLC. Drug and metabolite concentrations were determined using a Waters HPLC system (Waters Inc., Milford, MA). The system consisted of two Waters 510 pumps with Pump Control Module, a Waters 717plus auto-sampler, a Waters 996 Photodiode Array Detector, a Waters Xterra C_{18} reversed phase column (5 μm, 4.6 x 250 mm) equipped with guard column, and computer with Waters Empower software. The aqueous mobile phase (Solvent A) was 10 mM ammonium acetate pH 8.2 with triethylamine, and the organic mobile phase (Solvent B) was acetonitrile.

Elution conditions for BDCRB, TCRB and their aglycones were isocratic at 42%B with detection at 298.9 nm. The retention time (RT) was 6 min for the parent compounds and 11 - 12 min for the aglycones. Maribavir, its aglycone, and its n-dealkylated metabolite were eluted with a 2% per minute gradient from 30% to 54%B with detection at 307.1 nm, and the RTs were 4.1, 12.6 and 2.6 min, respectively. FTCRI and its aglycone were monitored at 301.2 nm and eluted with a 2% per min gradient from 61% to 81%B to yield 4.2 and 9 min RT. Adenosine and adenine were monitored at 261.4 nm and eluted isocratically with 4%B to yield RT of 5.7 and 4.2 min, respectively. Inosine and hypoxanthine were monitored at 251.6 nm and eluted isocratically with 2%B to yield RT of 5.7 and 4.7 min, respectively. Thymidine and thymine were eluted under identical conditions and monitored at 268.2 nm to yield 3.5 and 4.9 minute RT, respectively. Verapamil was eluted with a 2% per minute gradient from 20% to 50%B and detected by a Waters 474 fluorescence detector set at excitation and emission

wavelengths of 227 nm and 308 nm, respectively. The injection volume and flow rate were 50 μL and 1.0 mL/min, respectively, in all cases.

Nucleosides and aglycones were prepared by serial dilution of known concentrations in the same buffers and quenching solutions used for the reactions, and standard curves were analyzed with the appropriate HPLC method. The limit of detection (LOD) was defined as three times the standard deviation (SD) of three independent determinations of 12.5 μM standards. The LOD for BDCRB aglycone, TCRB aglycone, maribavir aglycone, hypoxanthine, adenine, and FTCRI aglycone was 1.8, 2.0, 1.1, 0.64, 0.72 and 2.4 μM, respectively.

Data Analysis. Initial metabolite appearance rates, v_0, were plotted as a function of substrate concentration, [S], and K_m and V_{max} were determined by nonlinear data fitting with WinNonlin 4.1 (Pharsight Corporation, Mountain View, CA) to the Michaelis-Menten equation. The catalytic rate constant, k_{cat}, for pure enzyme reactions was determined from $V_{max}/[E]$.

Data from Caco-2, human liver microsome and pure enzyme reactions are reported as mean ± SD from three independent experiments with data from each experiment determined in triplicate. Statistical significance was assessed by two-tailed unpaired t-tests with GraphPad Prism 4.02.

Molecular Modeling. A series of molecular modeling simulations was performed to probe the substrate specificity of hOGG1 and to attempt to understand the unique mechanism by which hOGG1 metabolizes nucleoside drugs. Molecular Operating Environment (MOE) version 2004.03 (Chemical Computing Group, Montreal, Quebec) was employed for docking simulations between native hOGG1 (PDB code 1KO9[4]) and

three nucleoside analogs—BDCRB, maribavir and guanosine. Hydrogen atoms were added to the crystal structure and minimized with the MMFF94x forcefield to a gradient of 0.05 Kcal mol^{-1} $Å^{-1}$ while keeping the heavy atoms fixed. Ligand molecules were built with MOE and minimized with the MMFF94x forcefield to a gradient of 0.05 Kcal mol^{-1} $Å^{-1}$. Minimized ligands were docked using MOE-Dock and the simulated annealing search algorithm for 25 runs with 6 cycles per run and 8000 iterations per cycle at an initial temperature of 1000 K.

None of the resulting guanosine conformations achieved proximity to the binding pocket of hOGG1 and therefore were not considered suitable for MD simulation. To confirm that absence of a suitable guanosine conformation was not a limitation of using only 25 runs, one additional run was performed using the previous parameters but a new starting conformation obtained by alignment of guanosine with the BDCRB conformation selected for MD simulation. This simulation yielded corroborative results.

Molecular dynamics simulations were performed with GROMACS 3.2 (Berendsen et al., 1995; Lindahl et al., 2001) and the Gromacs force field in a NVT (canonical) environment. Protonation state of specific residues was assigned automatically by the software. Individual ligand/protein complexes obtained from the docking results were soaked in a triclinic water box and minimized using a steepest descent algorithm to remove bad van der Waals contacts. The system was then equilibrated via a 20 ps MD simulation at 300°K with restrained ligand/protein complex atoms. Finally, a 500 ps simulation was performed at 300°K with a time step of 2 fs and hydrogen atoms constrained with a LINCS algorithm. Visualization of the dynamics trajectories was performed with the VMD software package, version 1.8.3 (Humphrey et

al., 1996). All calculations were performed on a RM 3GHz Pentium IV running Linux Fedora Core 3. The pKa values of some nucleoside analogs were determined using the ACD/pKa Database 6.0 (Advanced Chemistry Development, Toronto, Canada).

Results

Metabolism by First-Pass Models. Caco-2 cell homogenates and human liver microsomes were used as intestinal and hepatic surrogates to initially investigate the metabolism of BDCRB. Inosine and verapamil, serving as positive controls, produced expected results when tested for metabolism by Caco-2 homogenate and human liver microsomes (Table 1). These initial studies demonstrated that BDCRB was metabolized by Caco-2 homogenate but not by liver microsomes, whereas, in marked contrast, maribavir was not metabolized by either system.

Further characterization of BDCRB metabolism kinetics by Caco-2 homogenate showed that the optimal protein concentration was 0.15 mg/mL (Fig. 1A), and the reaction was linear through 8 min (Fig. 1B). The subsequent concentration-dependence study yielded a plateau in reaction velocity with increasing BDCRB concentration (Fig. 1C), thereby allowing calculation of K_m and V_{max} via nonlinear data fitting (Table 2). That BDCRB metabolism exhibited Michaelis-Menten kinetics in Caco-2 homogenate but was not metabolized by liver microsomes suggested that enzymes other than cytochrome P450 were involved in BDCRB metabolism.

Metabolism by Caco-2 Cell Fractions. To determine the subcellular localization of the enzyme activity responsible for BDCRB glycosidic bond cleavage, the kinetics of BDCRB metabolism were analyzed in 600 g nuclear pellet and supernatant fractions of Caco-2 cell homogenate (Table 2). The catalytic efficiency (V_{max}/K_m) of glycosidic bond cleavage in the supernatant fraction was 2-fold greater than that in the nuclear fraction, albeit not statistically significant. Hence, DNA microarrays were used to search for potentially responsible nuclear and soluble enzymes.

Intestinal Gene Expression. Gene expression data were obtained from samples of Caco-2 cells, human duodenum, jejunum, ileum and colon using Affymetrix U95Av2 GeneChips®, and the data were deposited under GEO series accession number GSE1862[3]. Genes that encode nucleoside-relevant enzymes, including glycosylases and phosphorylases, were queried for those statistically present in at least one sample according to the absolute detection call significance level of 0.05. These results were then queried for enzymes capable of N-glycosidic bond cleavage according to published mechanisms and substrates. Figure 2 illustrates the resulting set of 15 genes. Five of these enzymes were available for testing—hOGG1, mMPG, hPNP, hTP and E. coli TGT.

Figure 2 reveals the large degree of expression variability for these five genes in Caco-2 cells and intestinal tissues. OGG1 (EC 4.2.99.18[5]) was present in almost all samples, but expression was highest in Caco-2 cells and duodenum. MPG (EC 3.2.2.21[6], also known as AAG) was found to be statistically present in one Caco-2 sample and one colon sample (accession numbers GSM32836[7] and GSM32859[8], respectively), but this was possibly a limitation of the statistics employed by microarray analysis, since mean MPG expression levels appeared high relative to many other spots on the chip in all Caco-2, jejunum and colon samples. PNP (EC 2.4.2.1[9]) was expressed highly in duodenum and moderately in Caco-2 cells, and its pyrimidine counterpart—TP (EC 2.4.2.4[10])—was expressed moderately in all intestinal segments. TGT (EC 2.4.2.29[11]) expression was high in Caco-2 samples but was seemingly absent from intestinal tissues.

Metabolism by Selected Enzymes. Based upon these observations and availability, hOGG1, mMPG, hPNP, hTP and *E. coli* TGT were investigated for their ability to metabolize BDCRB. Time course studies revealed that the positive controls, inosine and

thymidine, were metabolized by hPNP and hTP, respectively, while BDCRB and maribavir were not (Table 3). Likewise, TGT did not metabolize either BDCRB or maribavir. BDCRB N-glycosidic bond cleavage was observed ($p < 0.0001$), however, in the presence of mMPG and hOGG1, while maribavir glycosidic bond cleavage was not. Further testing of hOGG1 substrate specificity indicated that the TCRB was also a substrate ($p < 0.0001$), while the indole analog, FTCRI, and the natural nucleosides adenosine, inosine and guanosine were not. K_m and V_{max} were calculated via nonlinear data fitting (Table 4), which demonstrated that the catalytic efficiency of TCRB metabolism by hOGG1 was roughly one half that of BDCRB.

Molecular Modeling. Molecular dynamics simulations were performed using the native hOGG1 crystal structure coordinates to elucidate a mechanism that could potentially explain nucleoside analog metabolism. Simulations were performed with BDCRB, maribavir and guanosine because the former is a substrate and the latter two are not. These substrates were first docked to the previously reported hOGG1 active site (Bjoras et al., 2002; Norman et al., 2003) to identify lowest energy binding conformations, from which the substrates underwent MD simulations. Snapshots (Figure 3) were taken at different stages of the MD simulations to demonstrate the most stable and, hence, most representative interactions between the ligands and the hOGG1 active site. The binding energy of BDCRB was -11.989 kJ/mol. Figure 3A shows hydrogen bonds formed between the Ser^{320} hydroxyl group and the BDCRB N-3 (2.85 Å) and between His^{270} and the BDCRB ribose oxygen (3.61 Å). This figure also shows that Phe^{319} has rotated approximately 90° to form pi-pi bonds with the benzimidazole moiety of BDCRB—an interaction that was maintained throughout the MD simulation. Figure 3B shows a

hydrogen bond formed between Asn^{149} and the 2′-OH of BDCRB (2.42 Å) and the distance from C1′ of BDCRB to the Lys^{249} nitrogen (4.58 Å), which is correctly placed for nucleophilic attack on the anomeric carbon. During the simulation, the core hydrogen bond between Asn^{149} and Lys^{249} is disrupted (Bjoras et al., 2002; Norman et al., 2003) and reformed between Asn^{149} and the 2′-OH. While within range of nucleophilic attack by Lys^{249}, BDCRB was stabilized by the hydrogen bond to His^{270} (3.68 Å). Maribavir achieved even greater binding energy than BDCRB, -19.278 kJ/mol. Figure 3C shows that maribavir was stabilized by multiple hydrogen bonds to the 2′-OH and 3′-OH. The lack of experimentally observed catalysis toward maribavir, however, was elucidated by the fact that the closest distance achieved between the maribavir anomeric carbon and the Lys^{249} nitrogen was 5.84 Å. Furthermore, the hydrogen bond to Asn^{149} and hindrance by the 2′-OH prevent catalytic access to the anomeric carbon of BDCRB (Figure 3D). The negative control guanosine did not achieve an energetically favorable binding to the OGG1 active site (-2.281 kJ/mol). Guanosine actually moved out of the active site over the course of the simulation, and Figure 3E shows the average distance achieved between Lys^{249} and C1′, 6.87 Å. Additionally, Lys^{249} and the base were on the same side of the sugar plane, so nucleophilic attack would not occur regardless of proximity.

Discussion

The selective N-glycosidic bond cleavage of BDCRB relative to maribavir by Caco-2 cell homogenates challenged us to identify enzymes that may be responsible. Function-based sorting of global gene expression data from Caco-2 cells and human intestinal tissues yielded 15 enzymes as possible candidates. This list was likely incomplete, as our stringent microarray data analysis ran the risk of falsely eliminating genes that were actually expressed at moderate levels. Such false elimination could be due to inadequate probe design or to lack of statistical significance over background. Another limitation of our study was the chip itself; as this was an older model array, it had only 12,000 gene probes that represented just one third of the human genome. Hence, additional BDCRB-metabolizing enzymes may exist, but we were nevertheless able to identify two.

Kinetic characterization of BDCRB metabolism by hOGG1 and mMPG permitted comparison with reported endogenous substrates of these enzymes. For example, the k_{cat}/K_m for BDCRB glycosidic bond cleavage by MPG (Table 4) was about 100-fold lower than the $1.5 \cdot 10^5$ $M^{-1} \cdot s^{-1}$ reported for cleavage of hypoxanthine from a double-stranded 25-mer DNA molecule (Miao et al., 1998; Xia and O'Connor, 2001) or from the free nucleoside inosine by hPNP (catalytic efficiency of $1.4 \cdot 10^5$ $M^{-1} \cdot s^{-1}$ in our experiments). This decreased efficiency of BDCRB N-glycosidic bond cleavage is likely due to non-optimal active site conformation in the absence of DNA binding. Dramatic active site changes that occur upon DNA binding to glycosylases suggest that DNA glycosylases have evolved for catalytic efficiency in the presence of DNA (Bjoras et al., 2002), with the exception of uracil DNA glycosylase (UDG), which has been shown to

efficiently cleave the glycosidic bond of free deoxyuridine (Jiang and Stivers, 2001). Although k_{cat}/K_m ratios indicated that BDCRB was metabolized only 6% as efficiently as endogenous DNA substrates of OGG1 and MPG, such inefficiency could be moot when considering the additive capacity (V_{max}) of DNA repair enzymes that results from their ubiquity and overlapping substrate specificity. The implication of glycosylases in drug metabolism therefore warrants further attention.

From a drug delivery standpoint, metabolism is most important in first-pass tissues. Our observation of OGG1 and MPG expression in human intestine (Figure 2) coupled with reports of their expression in human liver (Lash et al., 2000) suggests that these enzymes may play a significant role in BDCRB metabolism *in vivo*. In addition, a recent report that OGG1 knockout mice accumulated DNA damage in lung, small intestine and liver but not brain, spleen or kidney suggested functional presence of OGG1 in the aforementioned first-pass organs (Russo et al., 2004). As MPG and OGG1 are localized at the subcellular level to the nucleus and mitochondria (Nishioka et al., 1999), we assessed BDCRB N-glycosidic bond cleavage in Caco-2 nuclear and 600 g supernatant fractions to acquire evidence of the involvement of these enzymes in BDCRB metabolism. Metabolic activity was present in both the supernatant and nuclear fractions, suggesting metabolism by both nuclear and mitochondrial variants of MPG and OGG1. A dot blot of the fractions (see Supplemental Data) revealed nuclear contamination of the supernatant fraction, albeit minimal, which suggested that metabolism in the supernatant could have been due to nuclear enzymes. If nuclear enzymes alone were responsible, however, the observed V_{max}/K_m ratio in the supernatant fraction would have been lower than the nuclear fraction since those enzymes would be expected to be present at far

higher concentrations in the nuclear fraction. As that was not the case, we therefore assert that non-nuclear BDCRB-metabolizing enzymes must have been present in the supernatant, and mitochondrial MPG and OGG1 may explain such observations. The concept of drug metabolism by nuclear enzymes is nevertheless noteworthy, since many viral proteins that are potential drug targets localize to the nucleus. Such co-localization with potential drug targets in addition to reports of the promiscuity of these enzymes (O'Brien and Ellenberger, 2004b; O'Brien and Ellenberger, 2004a) implies a potentially significant role for these enzymes in nucleoside drug metabolism.

How can enzymes that normally act on double-stranded DNA (dsDNA) substrates act on free nucleosides? A series of explanations based on features of the enzyme and features of the ligand itself can be gleaned from MD simulations with hOGG1. The first noteworthy enzyme feature is Phe^{319}, which is reported to sterically crowd the binding pocket in the absence of a dsDNA substrate. Binding of hOGG1 to dsDNA initiates a conformational change in Phe^{319} that allows binding site access to the damaged base (Bjoras et al., 2002). Though this conformational change was believed to not occur in the absence of dsDNA binding, our MD simulations indicated that Phe^{319} rotated about 90° to form stabilizing pi-pi interactions with both BDCRB and maribavir.

Another important enzyme feature was His^{270}. With dsDNA substrates, His^{270} forms a hydrogen bond to the 5′-phosphate group of the damaged base (Bjoras et al., 2002). Similarly, His^{270} established a hydrogen bond with the ribose oxygen of BDCRB, providing ideal support for nucleophilic attack of C1′ by Lys^{249}, a third critical enzyme feature. Previous reports suggest that Lys^{249} becomes armed for nucleophilic attack via disruption of its hydrogen bond with Asn^{149} (Bjoras et al., 2002). With this knowledge,

we noted consistency between our theoretical and experimental observations—BDCRB conformations throughout the MD simulation permitted disruption of the Asn^{149}-Lys^{249} hydrogen bond (Figure 3B), while maribavir and guanosine did not. Such disruption would allow Lys^{249} to freely catalyze breakdown of the BDRCB glycosidic bond.

A recent mutation study provided evidence to suggest that Lys^{249} attack occurs subsequent to glycosidic bond cleavage (Norman et al., 2003). Likewise, studies with PNP indicated that the nucleophile, a phosphate ion, was only required to stabilize the resulting reaction intermediate (Kline and Schramm, 1993; Kline and Schramm, 1995; Erion et al., 1997; Bennett et al., 2003). If the role of Lys^{249} is to stabilize the reaction intermediate, then what event initiates glycosidic bond cleavage? One possibility, elucidated by a recent study with MPG, is protonation of the substrate's imidazole nitrogen (O'Brien and Ellenberger, 2003). This is consistent with the mechanism reported for nucleoside catalysis by acid (Zoltewicz et al., 1970) and by PNP (Bennett et al., 2003).

Experimental and theoretical observations agree with this hypothesis of a protonatable N-3. Table 3 indicates that only BDCRB and TCRB were substrates of hOGG1, and these two compounds had the highest N-3 pK_a, about 5.5, of the seven compounds tested. The N-3 of maribavir is significantly less protonatable with a pK_a of about 3.5, and the N-3 of FTCRI has been replaced by carbon, which effectively reduces its pK_a by 7 units. The pK_a of the analagous N-7 nitrogen of inosine, adenosine and guanosine is 1.2, 1.0 and 2.2, respectively (Dawson, 1960). Inspection of molecular dynamics simulations also confirmed that theoretical observations were consistent with this "protonatability" hypothesis, shown by the presence of a proton donor residue,

Ser^{320}, within 2.85 Å of the BDCRB N-3 (Figure 3A). Maribavir establishes the same interaction during the dynamics experiment, but it appears to be less stable. Guanosine, on the other hand, did not interact with Ser^{320} during the simulations. This apparent requirement for a very electronegative atom at the 2- position may explain why no free nucleoside substrates have been observed for hOGG1 to date. We previously hypothesized that N-3 protonation was involved in enzymatic N-glycosidic bond cleavage and therefore manipulated N-3 to design nucleoside analogs with more stable glycosidic bonds (Williams, 2004a; Williams, 2004b; Williams et al., 2004). One final feature of the nucleoside substrates that can explain how DNA glycosylases catalyze nucleosides is that unlike dsDNA, which must be processed by means of a nucleotide flipping mechanism that "flips" bases out of the strand and into the binding pocket (Slupphaug et al., 1996; McCullough et al., 1999; Lau et al., 2000; Dodson and Lloyd, 2002), free nucleosides have facile access to the active site.

In summary, we have identified two enzymes that metabolize the glycosidic bond of the potent antiviral nucleoside, BDCRB, and its homolog TCRB. The responsible enzymes, OGG1 and MPG, are both DNA glycosylases—a large family of enzymes whose endogenous role is to extract from DNA a wide variety of damaged bases that include UV photoadducts, mismatches, and alkylated or oxidized bases. Molecular modeling studies suggested that the mechanism of glycosidic bond cleavage by hOGG1 is similar for damaged DNA and free nucleoside substrates. In light of numerous reports of the wide substrate specificity of OGG1 and MPG, this newfound addition to their promiscuity should be considered as a potential major barrier to effective delivery of

antiviral and anticancer nucleoside analogs. This discovery will be critical to the design of more stable nucleoside analogs in the future.

ACKNOWLEDGMENTS

We thank Dr. R. Chandrasekharan for thorough and critical evaluation of the manuscript, Dr. John D. Williams for synthesizing the BDCRB and maribavir aglycones and for significantly helpful discussions, Dr. Lynda S. Welage for unrestricted use of her HPLC system, Chi Ho Ngan for assistance with enzyme kinetic experiments, and Dr. Tun-Cheng Chien, Jack Hinkley, Kathy Borysko, Julie Breitenbach and Gloria Komazin for helpful discussions and supplying additional reagents.

References

Bennett EM, Li C, Allan PW, Parker WB and Ealick SE (2003) Structural basis for substrate specificity of Escherichia coli purine nucleoside phosphorylase. *J Biol Chem* **278:**47110-47118.

Berendsen HJC, van der Spoel D and van Drunen R (1995) GROMACS: A message-passing parallel molecular dynamics implementation. *Comp Phys Comm* **91:**43-56.

Birnie GD, Kroeger H and Heidelberger C (1963) Studies of Fluorinated Pyrimidines. Xviii. The Degradation of 5-Fluoro-2'-Deoxyuridine and Related Compounds by Nucleoside Phosphorylase. *Biochemistry* **13:**566-572.

Biron KK, Harvey RJ, Chamberlain SC, Good SS, Smith AA, 3rd, Davis MG, Talarico CL, Miller WH, Ferris R, Dornsife RE, Stanat SC, Drach JC, Townsend LB and Koszalka GW (2002) Potent and selective inhibition of human cytomegalovirus replication by 1263W94, a benzimidazole L-riboside with a unique mode of action. *Antimicrob Agents Chemother* **46:**2365-2372.

Bjoras M, Seeberg E, Luna L, Pearl LH and Barrett TE (2002) Reciprocal "flipping" underlies substrate recognition and catalytic activation by the human 8-oxo-guanine DNA glycosylase. *J Mol Biol* **317:**171-177.

Chulay J, Biron K, Wang L, Underwood M, Chamberlain S, Frick L, Good S, Davis M, Harvey R, Townsend L, Drach J and Koszalka G (1999) Development of novel benzimidazole riboside compounds for treatment of cytomegalovirus disease. *Adv Exp Med Biol* **458:**129-134.

Dawson RMC (1960) *Data for biochemical research*. Clarendon Press, Oxford.

Dodson ML and Lloyd RS (2002) Mechanistic comparisons among base excision repair glycosylases. *Free Radic Biol Med* **32:**678-682.

Erion MD, Stoeckler JD, Guida WC, Walter RL and Ealick SE (1997) Purine nucleoside phosphorylase. 2. Catalytic mechanism. *Biochemistry* **36:**11735-11748.

Good SS, Owens BS, Townsend LB and Drach JC (1994) The disposition in rats and monkeys of 2-bromo-5,6-dichloro-1-(β-D-ribofuranosyl)benzimidazole (BDCRB) and its 2,5,6-trichloro congener (TCRB). *Antiviral Res* **23:**103.

Hidalgo IJ, Raub TJ and Borchardt RT (1989) Characterization of the human colon carcinoma cell line (Caco-2) as a model system for intestinal epithelial permeability. *Gastroenterology* **96:**736-749.

Humphrey W, Dalke A and Schulten K (1996) VMD - Visual Molecular Dynamics. *J Molecular Graphics* **14:**33-38.

Jiang YL and Stivers JT (2001) Reconstructing the substrate for uracil DNA glycosylase: tracking the transmission of binding energy in catalysis. *Biochemistry* **40:**7710-7719.

Kern ER, Hartline CB, Rybak RJ, Drach JC, Townsend LB, Biron KK and Bidanset DJ (2004) Activities of benzimidazole D- and L-ribonucleosides in animal models of cytomegalovirus infections. *Antimicrob Agents Chemother* **48:**1749-1755.

Kline PC and Schramm VL (1993) Purine nucleoside phosphorylase. Catalytic mechanism and transition-state analysis of the arsenolysis reaction. *Biochemistry* **32:**13212-13219.

Kline PC and Schramm VL (1995) Pre-steady-state transition-state analysis of the hydrolytic reaction catalyzed by purine nucleoside phosphorylase. *Biochemistry* **34:**1153-1162.

Koszalka GW, Johnson NW, Good SS, Boyd L, Chamberlain SC, Townsend LB, Drach JC and Biron KK (2002) Preclinical and toxicology studies of 1263W94, a potent and selective inhibitor of human cytomegalovirus replication. *Antimicrob Agents Chemother* **46:**2373-2380.

Krosky PM, Underwood MR, Turk SR, Feng KW, Jain RK, Ptak RG, Westerman AC, Biron KK, Townsend LB and Drach JC (1998) Resistance of human cytomegalovirus to benzimidazole ribonucleosides maps to two open reading frames: UL89 and UL56. *J Virol* **72:**4721-4728.

Lash AE, Tolstoshev CM, Wagner L, Schuler GD, Strausberg RL, Riggins GJ and Altschul SF (2000) SAGEmap: a public gene expression resource. *Genome Res* **10:**1051-1060.

Lau AY, Wyatt MD, Glassner BJ, Samson LD and Ellenberger T (2000) Molecular basis for discriminating between normal and damaged bases by the human alkyladenine glycosylase, AAG. *Proc Natl Acad Sci U S A* **97:**13573-13578.

Lindahl E, Hess B and van der Spoel D (2001) GROMACS 3.0: A package for molecular simulation and trajectory analysis. *J Mol Mod* **7:**306-317.

Lorenzi PL, Landowski CP, Song X, Borysko KZ, Breitenbach JM, Kim JS, Hilfinger JM, Townsend LB, Drach JC and Amidon GL (2005) Amino acid ester prodrugs of 2-bromo-5,6-dichloro-1-(β-D-ribofuranosyl)benzimidazole enhance metabolic stability in vitro and in vivo. *J Pharmacol Exp Ther* **343:**883-90.

McCullough AK, Dodson ML and Lloyd RS (1999) Initiation of base excision repair: glycosylase mechanisms and structures. *Annu Rev Biochem* **68:**255-285.

Miao F, Bouziane M and O'Connor TR (1998) Interaction of the recombinant human methylpurine-DNA glycosylase (MPG protein) with oligodeoxyribonucleotides containing either hypoxanthine or abasic sites. *Nucleic Acids Res* **26:**4034-4041.

Nishioka K, Ohtsubo T, Oda H, Fujiwara T, Kang D, Sugimachi K and Nakabeppu Y (1999) Expression and differential intracellular localization of two major forms of human 8-oxoguanine DNA glycosylase encoded by alternatively spliced OGG1 mRNAs. *Mol Biol Cell* **10:**1637-1652.

Norman DP, Chung SJ and Verdine GL (2003) Structural and biochemical exploration of a critical amino acid in human 8-oxoguanine glycosylase. *Biochemistry* **42:**1564-1572.

O'Brien PJ and Ellenberger T (2003) Human alkyladenine DNA glycosylase uses acid-base catalysis for selective excision of damaged purines. *Biochemistry* **42:**12418-12429.

O'Brien PJ and Ellenberger T (2004a) Dissecting the broad substrate specificity of human 3-methyladenine-DNA glycosylase. *J Biol Chem* **279:**9750-9757.

O'Brien PJ and Ellenberger T (2004b) The Escherichia coli 3-methyladenine DNA glycosylase AlkA has a remarkably versatile active site. *J Biol Chem* **279:**26876-26884.

Russo MT, De Luca G, Degan P, Parlanti E, Dogliotti E, Barnes DE, Lindahl T, Yang H, Miller JH and Bignami M (2004) Accumulation of the oxidative base lesion 8-

hydroxyguanine in DNA of tumor-prone mice defective in both the Myh and Ogg1 DNA glycosylases. *Cancer Res* **64:**4411-4414.

Scheffczik H, Savva CG, Holzenburg A, Kolesnikova L and Bogner E (2002) The terminase subunits pUL56 and pUL89 of human cytomegalovirus are DNA-metabolizing proteins with toroidal structure. *Nucleic Acids Res* **30:**1695-1703.

Scholz B, Rechter S, Drach JC, Townsend LB and Bogner E (2003) Identification of the ATP-binding site in the terminase subunit pUL56 of human cytomegalovirus. *Nucleic Acids Res* **31:**1426-1433.

Slupphaug G, Mol CD, Kavli B, Arvai AS, Krokan HE and Tainer JA (1996) A nucleotide-flipping mechanism from the structure of human uracil-DNA glycosylase bound to DNA. *Nature* **384:**87-92.

Sun D, Lennernas H, Welage LS, Barnett JL, Landowski CP, Foster D, Fleisher D, Lee KD and Amidon GL (2002) Comparison of human duodenum and Caco-2 gene expression profiles for 12,000 gene sequences tags and correlation with permeability of 26 drugs. *Pharm Res* **19:**1400-1416.

Townsend LB, Devivar RV, Turk SR, Nassiri MR and Drach JC (1995) Design, synthesis, and antiviral activity of certain 2,5,6-trihalo-1-(beta-D-ribofuranosyl)benzimidazoles. *J Med Chem* **38:**4098-4105.

Townsend LB and Drach JC (1992) Benzimidazole ribonucleosides: design, synthesis, evaluation, and mode of action., in: *Fifth Internat Conf Antiviral Res*, pp Abstracts 12, 105, 107, 108, 110, Vancouver, B.C.

Townsend LB, Gudmundsson KS, Daluge SM, Chen JJ, Zhu Z, Koszalka GW, Boyd L, Chamberlain SD, Freeman GA, Biron KK and Drach JC (1999) Studies designed

to increase the stability and antiviral activity (HCMV) of the active benzimidazole nucleoside, TCRB. *Nucleosides Nucleotides* **18:**509-519.

Underwood MR, Harvey RJ, Stanat SC, Hemphill ML, Miller T, Drach JC, Townsend LB and Biron KK (1998) Inhibition of human cytomegalovirus DNA maturation by a benzimidazole ribonucleoside is mediated through the UL89 gene product. *J Virol* **72:**717-725.

Williams JD, Chen J. J., Drach, J. C., and Townsend L. B. (2004a) Design, synthesis, and antiviral activity of certain 3-substituted 2,5,6-trichloroindole nucleosides. *J Med Chem***:**In Press.

Williams JD, Drach JC and Townsend LB (2004) Synthesis and antiviral evaluation of some novel tricyclic pyrazolo[3,4-b]indole nucleosides. *Nucleosides Nucleotides Nucleic Acids* **23:**805-812.

Williams JD, Ptak, R. G., Drach, J. C., and Townsend, L. B. (2004b) Synthesis, antiviral activity, and mode of action of some 3-substituted 2,5,6-trichloroindole 2'- and 5'-deoxyribonucleosides. *J Med Chem***:**In Press.

Xia L and O'Connor TR (2001) DNA glycosylase activity assay based on streptavidin paramagnetic bead substrate capture. *Anal Biochem* **298:**322-326.

Zoltewicz JA, Clark DF, Sharpless TW and Grahe G (1970) Kinetics and mechanism of the acid-catalyzed hydrolysis of some purine nucleosides. *J Am Chem Soc* **92:**1741-1749.

FOOTNOTES

This work was made possible by NIH grant numbers R01-GM37188 and P01-AI46390. PLL was supported by training grant GM07767 NIGMS. The contents are solely the responsibility of the authors and do not necessarily represent the official views of NIGMS.

[1]Current address: Genomics and Bioinformatics Group, Laboratory of Molecular Pharmacology, National Cancer Institute, National Institutes of Health, Bethesda, Maryland.

[2]Current address: Institute for Biochemistry and Molecular Biology, University of Berne, Switzerland.

[3]Gene Expression Omnibus = GEO Accession # GSE1862

[4]Research Collaboratory for Structural Bioinformatics Protein Databank = PDB # 1KO9

[5]Enzyme Collection Number = 4.2.99.18

[6]Enzyme Collection Number = 3.2.2.21

[7]Gene Expression Omnibus = GEO Accession # GSM32836

[8]Gene Expression Omnibus = GEO Accession # GSM32859

[9]Enzyme Collection Number = 2.4.2.1

[10]Enzyme Collection Number = 2.4.2.4

[11]Enzyme Collection Number = 2.4.2.29

Figure Legends

FIG. 1. BDCRB glycosidic bond cleavage by Caco-2 cell homogenate. (A) Rate of BDCRB aglycone appearance as a function of Caco-2 protein concentration following addition of 1 mM BDCRB and sampling at 20 min. (B) Time course of BDCRB aglycone appearance with 0.15 mg/mL Caco-2 protein and 1 mM BDCRB. The reaction was linear through 8 min. (C) Substrate concentration dependence to determine K_m and V_{max}. Rate of BDCRB aglycone formation was determined following addition of a range of substrate concentrations to 0.15 mg/mL Caco-2 protein with sampling at 8 min.

FIG. 2. Gene expression of enzymes in human intestinal tissues and Caco-2 cells that cleave N-glycosidic bonds. Affymetrix model U95Av2 GeneChips® were employed to analyze total RNA from Caco-2 cells grown 4 days (undifferentiated) or 16 days (differentiated) and from human duodenum, jejunum, ileum and colon tissues. The resulting data (GEO accession # GSE1862[3]) was averaged and queried for glycosylases, phosphorylases and other nucleoside-relevant genes. The figure illustrates gene products documented to cleave glycosidic bonds and determined to be present by absolute detection calls at a significance level of 0.05.

FIG. 3. Molecular Modeling. Snapshots taken at different stages during molecular dynamics simulations to demonstrate interactions between the ligands BDCRB, maribavir and guanosine and residues of the native human 8-oxoguanine DNA glycosylase enzyme (PDB #1KO9[4]). (A) Hydrogen bonds formed from Ser^{320} to N-3 and His^{270} to the ribose oxygen of BDCRB (in yellow). The distance from C1′ of BDCRB to the Lys^{249} nitrogen

(in green). (B) Additional residues that form H-bonds to the ribose ring of BDCRB. (C) Hydrogen bonds formed between maribavir and residues of the OGG1 binding pocket. (D) The distance from C1′ of maribavir to Lys^{249}. (E) Residues interacting with guanosine.

DMD Fast Forward. Published on March 24, 2006 as DOI: 10.1124/dmd.105.009209
This article has not been copyedited and formatted. The final version may differ from this version.

TABLE 1

Aglycone formation measured by studies with 1st-pass models

Enzymatic System		$Metabolite_{obs}$ (nmol)	$Metabolite_{non\text{-}enzymatic}$ (nmol)
Caco-2 Cell Homogenate[a]			
	Inosine***	5.1 ± 0.6	< 0.003[b]
	BDCRB***	12 ± 1	0.18 ± 0.07
	Maribavir	< 0.006[b]	< 0.006[b]
Human Liver Microsomes[c]			
	Verapamil***	18 ± 2	0.14 ± 0.12
	BDCRB	0.19 ± 0.07	0.13 ± 0.04
	Maribavir	< 0.006[b]	< 0.006[b]

[a]Caco-2 cells were homogenized in Buffer C containing 0.5% Triton X-100. Protein was quantitated and homogenate was diluted to final 1 mg/mL in Buffer C, in which 200 μM substrate was also prepared prior to addition to the homogenate reaction. Reactions were quenched with ice-cold methanol at 0 and 60 min. Aglycone was quantitated by HPLC.

[b]Limit of detection, as no measurable aglycone was detected

[c]Human liver microsomes were diluted to final 150 μg/mL in 100 mM Tris, pH 7.4. Drug was prepared in NADPH regenerating solution, combined with microsomes at 200 μM, quenched at 0 and 60 min with ice-cold methanol and quantitated as above. All values are reported as mean ± SD (n=3).

***$p < 0.0001$ determined by 2-tailed t-tests comparing metabolite formed in the presence vs. absence of protein

TABLE 2

Kinetic parameters for N-glycosidic bond cleavage by Caco-2 whole cell homogenate and homogenized cell fractions

Substrate	K_m (mM)	V_{max} (nmol/min/mg)	V_{max}/K_m (µL/min/mg)
Caco-2 whole[a]			
Inosine	0.15 ± 0.02	16.7 ± 0.9	111 ± 21
BDCRB	14.1 ± 0.2	93 ± 11	6.6 ± 2.2
Caco-2 fractions[b]			
$BDCRB_{nuclear}$	0.36 ± 0.09	2.4 ± 0.2	6.7 ± 3.0
$BDCRB_{supernatant}$	2.9 ± 0.5	37 ± 3	12.8 ± 4.8

[a]Caco-2 cells were homogenized in Buffer C containing 0.5% Triton X-100. Protein was quantitated and homogenate diluted to 0.15 mg/mL in Buffer C, in which a range of substrate concentrations were also prepared. Reactions were started and quenched at 8 min with methanol. Aglycone was quantitated by HPLC, and resulting reaction rates were calculated and plotted as a function of initial substrate concentration. K_m and V_{max} were calculated by non-linear data fitting with WinNonlin 4.0.

[b]Following mechanical shearing with a Potter-Elvehjem homogenizer, Caco-2 cells were fractionated via centrifugation at 600 g for 10 min. Each fraction was brought to 0.5% Triton X-100 and homogenized, and reactions were performed and analyzed as above. All data are presented as mean ± SD (n=3).

DMD Fast Forward. Published on March 24, 2006 as DOI: 10.1124/dmd.105.009209
This article has not been copyedited and formatted. The final version may differ from this version.

TABLE 3

Aglycone formation measured by studies with selected enzymes

Enzymatic System[a]	$Metabolite_{obs}$ (nmol)	$Metabolite_{non\text{-}enzymatic}$ (nmol)
Purine Nucleoside Phosphorylase		
Inosine***	91 ± 3	0.08 ± 0.03
BDCRB	0.21 ± 0.05	0.19 ± 0.05
Maribavir	< 0.006[b]	< 0.006[b]
Thymidine Phosphorylase		
Thymidine***	104 ± 5	0.24 ± 0.03
BDCRB	0.16 ± 0.03	0.19 ± 0.05
Maribavir	< 0.006[b]	< 0.006[b]
tRNA-guanine Transglycosylase		
BDCRB	0.15 ± 0.03	0.14 ± 0.03
Maribavir	< 0.006[b]	< 0.006[b]
N-Methylpurine DNA Glycosylase		
BDCRB***	77 ± 4	0.18 ± 0.04
Maribavir	< 0.006[b]	< 0.006[b]
8-Oxoguanine DNA Glycosylase		
BDCRB***	63 ± 5	0.21 ± 0.06
Maribavir	< 0.006[b]	< 0.006[b]
TCRB***	37 ± 2	0.14 ± 0.03
FTCRI	0.19 ± 0.04	0.17 ± 0.03
Adenosine	0.52 ± 0.06	0.49 ± 0.04
Inosine	0.09 ± 0.04	0.10 ± 0.03
Guanosine	0.35 ± 0.02	0.39 ± 0.04

[a]Each enzyme was diluted to 3 μg/mL in appropriate reaction buffer, in which 200 μM substrate was also prepared. Reactions were aliquoted into methanol at 0 and 60 min. Aglycone was quantitated by HPLC, and resulting values are reported as mean ± SD (n=3).

[b]Limit of detection, as no measurable aglycone was detected

***$p < 0.0001$ determined by 2-tailed t-tests comparing metabolite formed in the presence vs. absence of enzyme

DMD Fast Forward. Published on March 24, 2006 as DOI: 10.1124/dmd.105.009209
This article has not been copyedited and formatted. The final version may differ from this version.

TABLE 4

Kinetic parameters for N-glycosidic bond cleavage by 8-oxoguanine DNA glycosylase (OGG1) and N-methylpurine DNA glycosylase (MPG)

Drug	K_m (mM)	V_{max} (μmol/min/mg)	k_{cat} (s^{-1})	k_{cat}/K_m (10^3 $M^{-1}s^{-1}$)
8-Oxoguanine DNA Glycosylase[a]				
BDCRB	4.2 ± 0.3	48 ± 4	29 ± 2	6.9 ± 1.7
TCRB	9.4 ± 3.2	68 ± 11	41 ± 7	4.6 ± 0.8
N-Methylpurine DNA Glysosylase[b]				
BDCRB	4.6 ± 0.2	62 ± 5	38 ± 3	8.3 ± 2.0

[a]8-oxoguanine DNA glycosylase and [b]N-methylpurine DNA glycosylase were diluted to 3 and 6 μg/mL in reaction buffer, respectively. A range of substrate concentrations were also prepared in this buffer, and reactions were started and quenched at 8 min with methanol. Aglycone was quantitated by HPLC, and resulting reaction rates were calculated and plotted as a function of initial substrate concentration. K_m and V_{max} were calculated by non-linear data fitting with WinNonlin 4.0. k_{cat} was calculated as $V_{max}/[E]$.

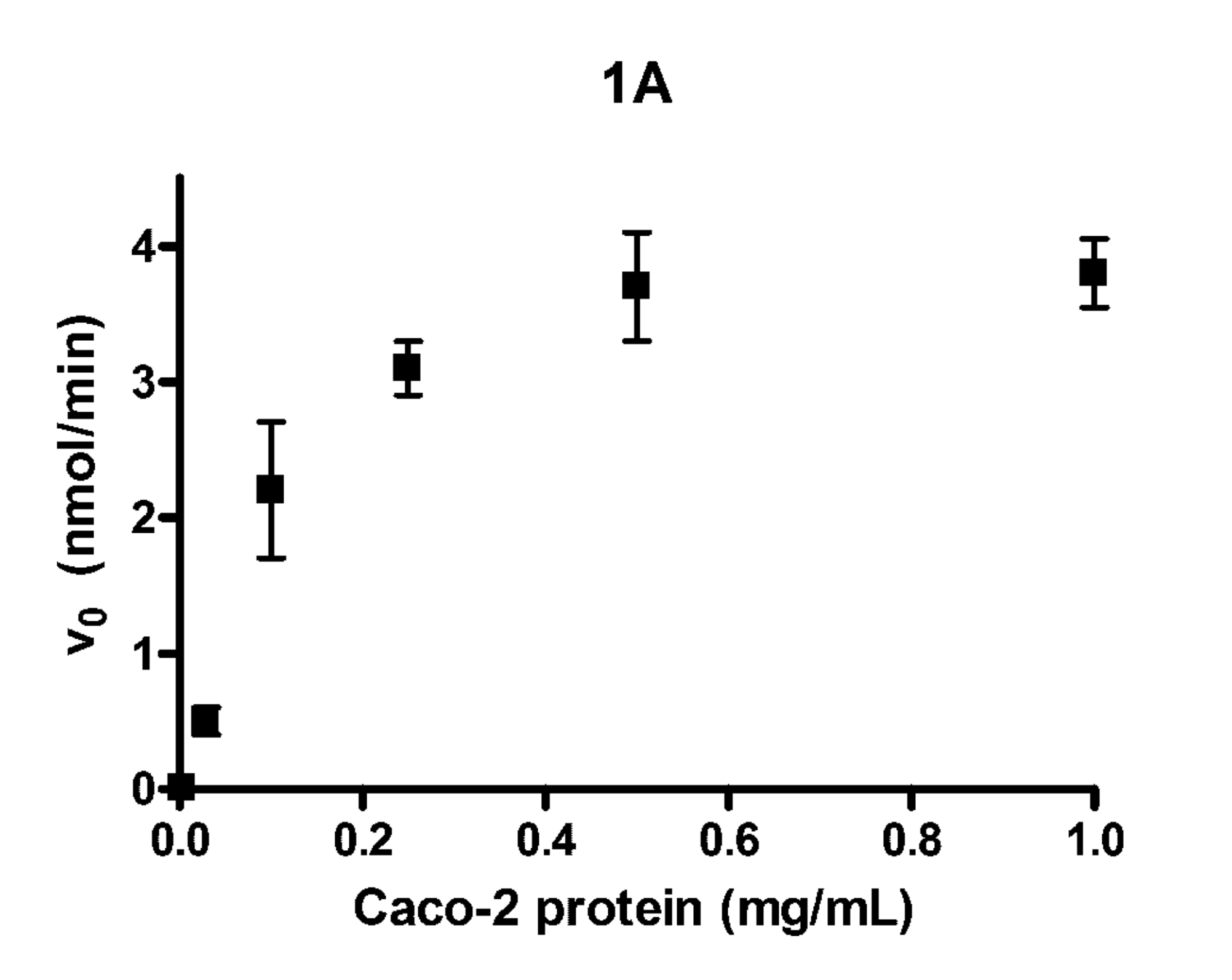
1A
4
3
2
1
0
v_0 (nmol/min)
0.0
0.2
0.4
0.6
0.8
1.0
Caco-2 protein (mg/mL)

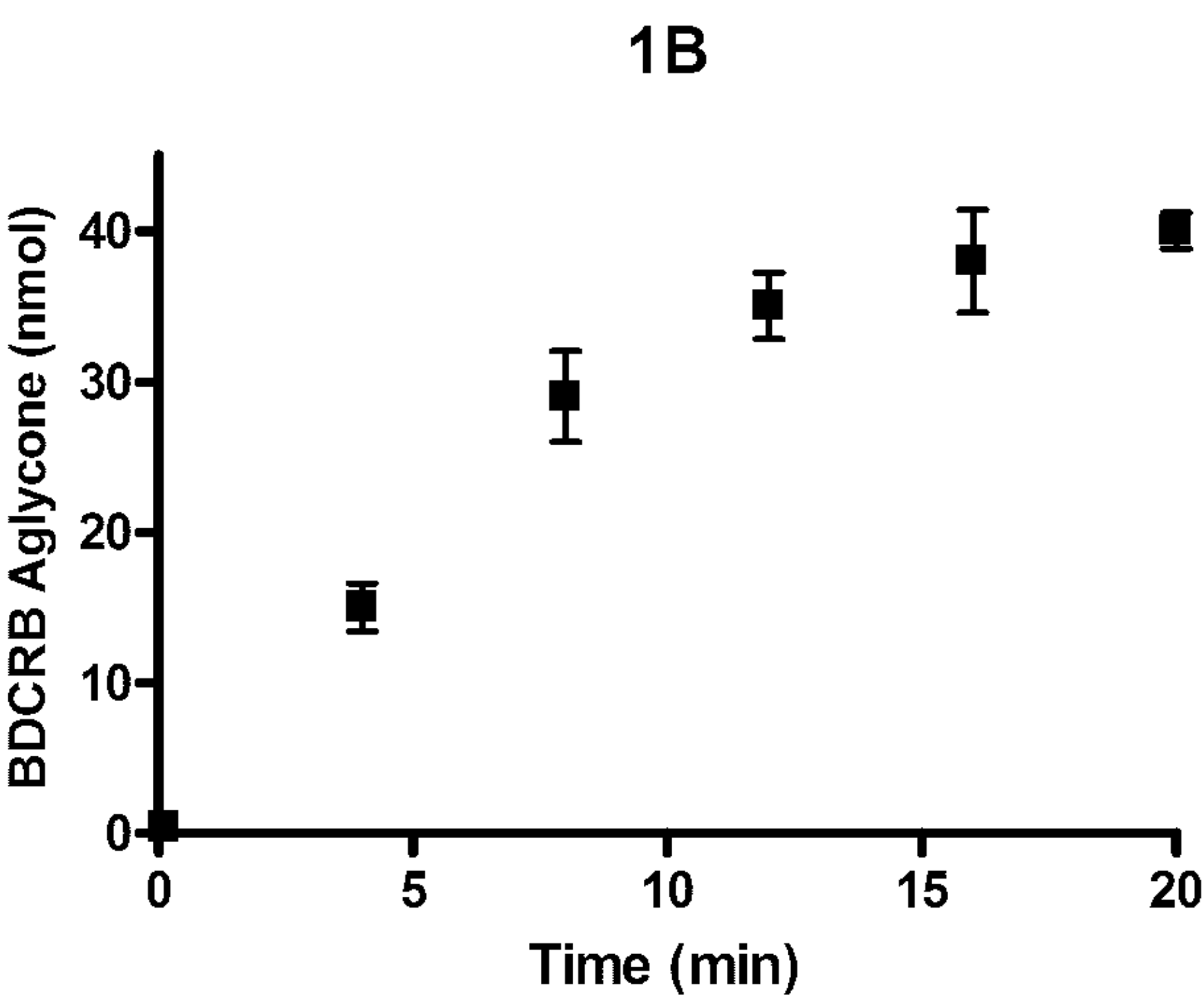
1B
BDCRB Aglycone (nmol)
40
30
20
10
0
0
5
10
15
20
Time (min)

1C

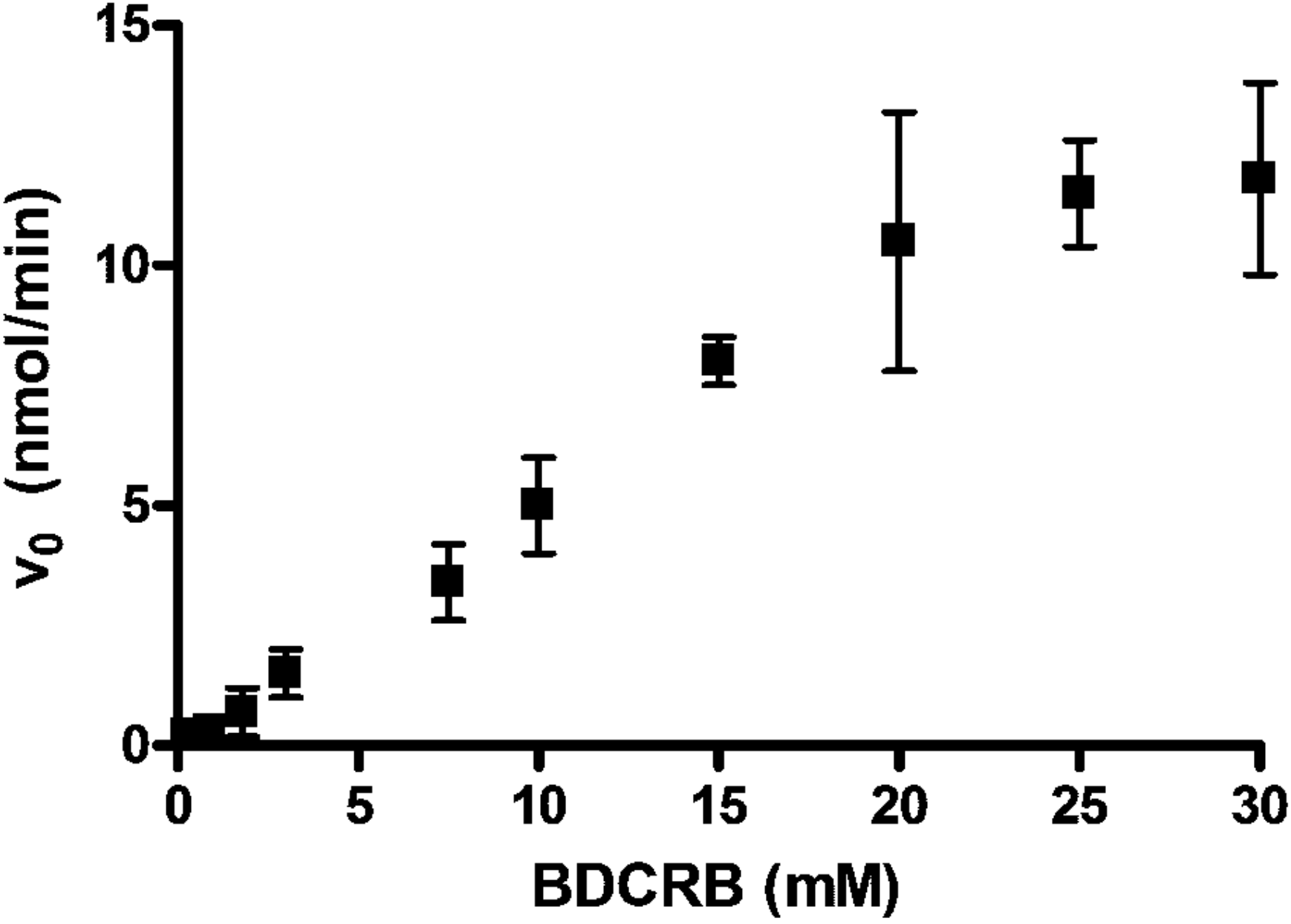

2

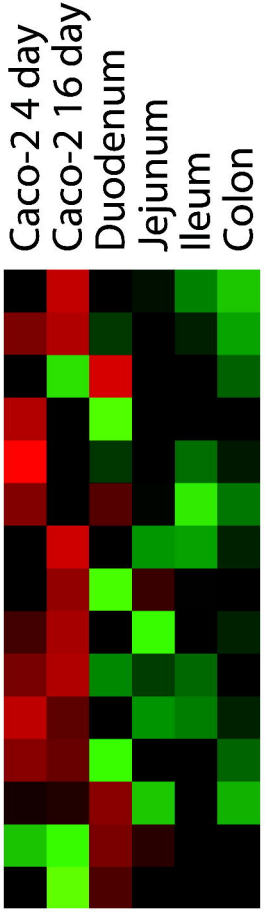

8-oxoguanine DNA glycosylase [OGG1]
APEX nuclease 1 [APEX1]
bone marrow stromal cell antigen 1 [BST1]
nth endonuclease III-like 1 [NTHL1]
polyribonucleotide nucleotidyltransferase [PNPase]
methyl-CpG binding domain protein 4 [MBD4]
E. coli mutY homolog [MUTYH]
N-methylpurine-DNA glycosylase [MPG]
thymine-DNA glycosylase [TDG]
tRNA-guanine transglycosylase [TGT]
uracil-DNA glycosylase [UDG]
methylthioadenosine phosphorylase [MTAP]
purine nucleoside phosphorylase [PNP]
thymidine phosphorylase [TP]
uridine phosphorylase [UP]

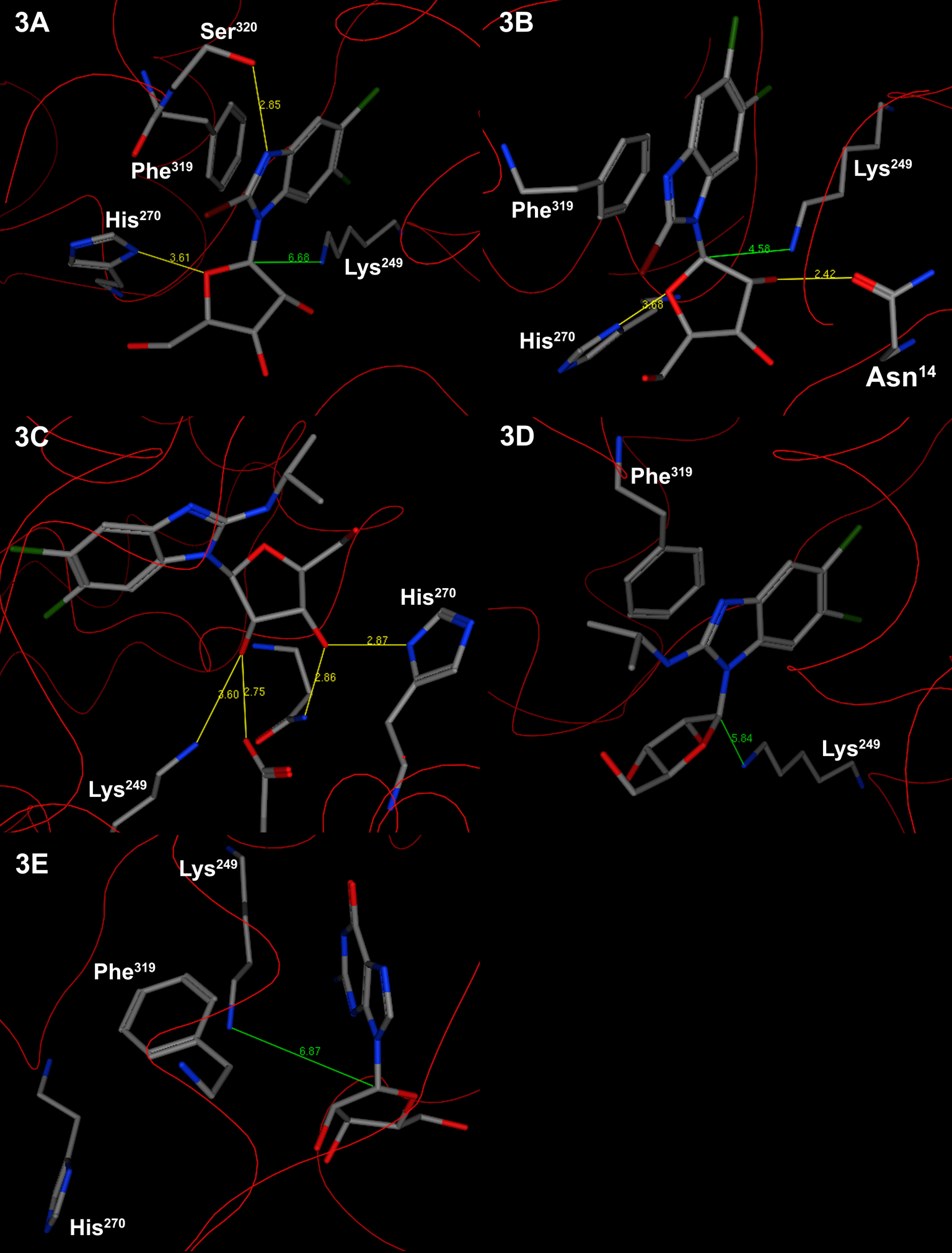
3A
Ser320
2.85
Phe319
His270
3.61
6.68
Lys249
3B
Phe319
Lys249
4.58
2.42
3.68
His270
Asn14
3C
His270
2.87
2.86
3.60
2.75
Lys249
3D
Phe319
5.84
Lys249
3E
Lys249
Phe319
6.87
His270